PROCEEDINGS OF SCIENCE

The trigger design for AdvCam

Leonid Burmistrov,[a,*] Matthieu Heller,[a] Luca Giangrande,[a] Tjark Miener,[a] Teresa Montaruli,[a] Iaroslava Bezshyiko,[d] Carlos Abellan Beteta,[d] Jorge Buces,[b] Dafne Martín-Domínguez,[b] Daniel Nieto,[b] María Molina Delicado,[b] Alejandro Pérez Aguilera,[b] Juan Abel Barrio,[b] Luis Ángel Tejedor Álvarez,[b] Andres Upegui Posada,[c] Tanguy Dietrich[c] and Quentin Berthet[c]

[a] *Département de Physique Nucléaire et Corpusculaire, Université de Genève, Faculté de Sciences, 1211 Genève 4, Switzerland*

[d] *Physik-Institute of the University of Zurich, Switzerland*

[b] *Institute of Particle and Cosmos Physics, Universidad Complutense de Madrid, Pza. Ciencias 1, Madrid E-28040, Spain*

[c] *Haute École du Paysage, d'Ingénierie et d'Architecture Rue de la Prairie 4 CH-1202 Genève, Switzerland*

E-mail: leonid.burmistrov@unige.ch

The AdvCam is a next-generation camera for the Large-Sized Telescopes of the Cherenkov Telescope Array Observatory, based on silicon photomultipliers. Its fully digital readout system enables the design of new, sophisticated trigger logic.

The Large-Sized Telescopes aim to cover the low-energy range of the cosmic gamma-ray spectrum, with a threshold starting at about 20 GeV, using the existing photomultiplier tube camera. The AdvCam, along with the new trigger logic, as shown by simulations, lowers the detectable energy threshold to 13 GeV.

The proposed trigger logic has a multilevel structure. The first level involves fast coincidences among small pixel regions at a rate of approximately 1 GHz, while the second level processes all camera pixels within an approximately 10-nanosecond time window. Different families of machine learning algorithms optimized for FPGAs form the second-level trigger. In this work, we consider two main approaches: Deep Neural Networks and Density-Based Spatial Clustering of Applications with Noise, both running with latencies below 1 microsecond at a 1 MHz rate. This work provides a detailed description of the trigger chain and its performance, as studied through simulation.

39th International Cosmic Ray Conference (ICRC2025)
15–24 July 2025
Geneva, Switzerland

ICRC 2025
The Astroparticle Physics Conference
Geneva July 15-24, 2025

*Speaker

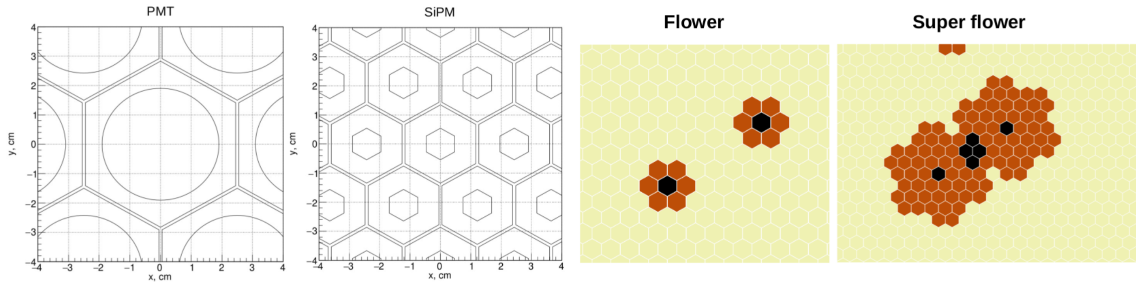

Figure 1: (**Left**): A close-up view of the PMT and SiPM-based cameras. The PMTs are round and have a diameter of ∼ 4 cm. The hexagonal outline around it shows the light guide interfaced to the PMT. The SiPMs and their light guides have a hexagonal shape. The flat-to-flat distance of the SiPM is approximately 2.2 cm. (**Right**): Pixel grouping patterns referred to as : flower and super-flower. The flower pattern consists of a central pixel, or seed (shown in black), with 6 surrounding pixels (total of 7 channels). The super-flower pattern consists of a central flower surrounded by 6 flowers (total of 49 channels).

1. Introduction

The Cherenkov Telescope Array Observatory (CTAO) [1] is the next-generation ground-based facility designed to detect high-energy gamma rays. It uses an array of telescopes to capture the Cherenkov light produced when gamma rays interact with Earth's atmosphere, as described in more detail [2]. CTAO will provide unprecedented sensitivity and precision in energy and direction reconstruction, helping to study extreme cosmic phenomena such as supernovae, neutron stars, black holes. CTAO is a powerful instruments for studying dark matter by searching for gamma-ray signals resulting from its annihilation or decay.

The CTAO will be built on two sites, one in the Northern hemisphere (La Palma, Spain) and one in the Southern hemisphere (Atacama Desert, Chile) to provide full coverage of the sky. The observatory consists of three types of telescopes, each optimized to detect gamma rays of different energies. **LSTs:** Large-Sized Telescopes, with a mirror diameter of 23 m, a low-energy threshold of about ∼20 GeV, and a field of view of 4.5°. **MSTs:** Medium-Sized Telescopes, with a mirror diameter of 12 m, a low-energy threshold of about ∼100 GeV, and a field of view of 8°. **SSTs:** Small-Sized Telescopes, with a mirror diameter of 4 m, a low-energy threshold of about ∼1 TeV, and a field of view of ∼ 9°.

2. SiPM camera

Reducing the energy threshold requires detecting a greater amount of Cherenkov light. Thus going for larger mirror dishes would decrease the energy threshold. However, the LST reaches the limits of mechanical lightness and agility required for rapid repositioning, while keeping the structure affordable to build. An alternative approach is to use light sensors with improved photo-detection efficiency (PDE). Modern Silicon Photomultiplier (SiPM) achieve a maximum PDE of about 70 %, which surpasses the theoretical limit of classical Photomultiplier Tubes (PMT). Additionally, the crosstalk is reduced to less than 5% while maintaining a PDE of around 70% [3]. SiPMs are already used in Cherenkov telescopes, such as SST-1M [4], Terzina [5, 6].

	Gamma on axis	Gamma diffuse	Proton	Electron
Energy, TeV	0.005 - 50	0.005 - 50	0.01 - 100	0.005 - 5
View cone, degree	0	6	10	6
Generation circle radius, m	800	1000	1500	1000

Table 1: Simulation parameters for different particle types. Each shower is reused 10 times with different impact parameters.

These factors motivate the AdvCam project [7], which aims to develop a SiPM-based camera for LST. The camera has four times more pixels (compared to current PMT camera) for the same field of view enabling finer image resolution (Figure 1, left panel). It is important to mention that the main challenge is that the increased PDE of SiPMs also increases their sensitivity to night sky background (NSB). Therefore, new triggering and filtering algorithms play an important role in enhancing sensitivity.

3. Simulation pipeline

Our study is based on Monte Carlo simulations of protons, gammas, and electrons. Their interactions with the atmosphere, including the initiation, development of extensive air showers and the propagation of Cherenkov light through the atmosphere, are simulated by Corsika 7.7 [8]. Ray-tracing, optical simulation of the telescope, and the electronics response are simulated using sim_telarray (2020-06-29 ver.) [9]. The NSB level is set to 268 MHz per AdvCam channel. We consider a 14-bit ADC with a 1.024 GHz waveform digitization frequency, 8.25 ADC counts per photoelectron (p.e.), and 3.94 ADC counts of electronic noise (RMS). The recorded waveform length is 75 points, corresponding to a ~73.2 ns time window.

We performed trigger-less simulations for four LSTs, requiring only a minimum number of p.e. to be detected by a single telescope, and considered a single pointing direction (20°, zenith and 180°, azimuth). The energy spectrum we simulate follows a $1/E^2$ distribution for each particle type. For proton rate estimation, we use two smoothly broken power-law models, taken from the DAMPE [10]. For the gamma rate estimation, we assume the Crab Nebula spectrum follows a modified log-parabola function, taken from [11]. Details of the simulation parameters are summarized in Table 1.

Protons are the dominant source of background and are indistinguishable from gamma rays at the trigger level. Considering a DAQ bandwidth of about 50 kHz, a minimum triggering threshold of 20 p.e. can be set. At low trigger thresholds, the NSB dominates the rates and can rapidly saturate the data acquisition system. Therefore, the main goal of the trigger is to separate proton/gamma showers from NSB.

4. Trigger logic

The fully digital readout of AdvCam enables a multi-level trigger hierarchy that allows a reduction of the detection energy threshold, while keeping a manageable rate for the data written to disk. This hierarchy splits into a low-level logic, hardware-based, including a Level 1 and a Level 2 Trigger, and a high-level logic, software-based, corresponding to the Level 3 Trigger (Figure 2).

Level 1 Trigger. The initial trigger stage, dubbed L1, is a digital sum computed at the Front-End-Boards (FEBs) in a real-time, 1 GHz, rate, on a group of 49 pixels, referred to, later in the text, as L1 trigger patches or super flower (Figure 1). L1 trigger patches overlaps, so that they are computed centered on each 7-pixel flower, leaving no dead or inefficient regions in the camera. A simple threshold cut is applied to the super flower digital sum, so that for each 7-pixel flower a L1 trigger signal is produced. A different use of the L1 signals will be done, depending on the chosen algorithm for the Level 2 Trigger.

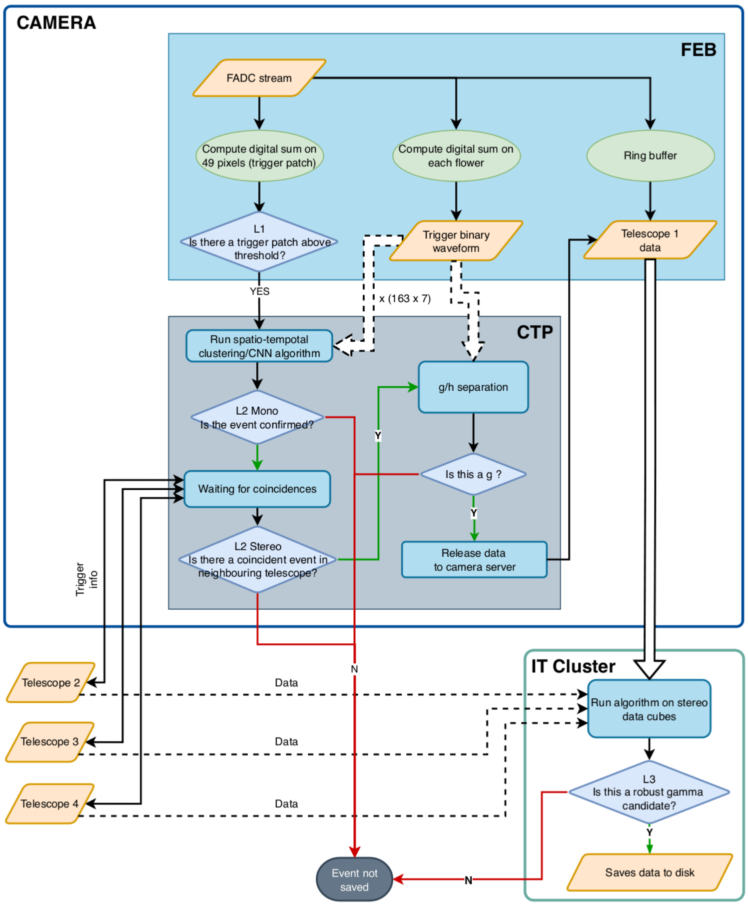

Figure 2: Trigger Flow Diagram.

Level 2 Trigger. The Level 2 trigger, dubbed L2, is performed at the Central Trigger Processor (CTP), a camera electronics subsystem involving a set of Field-Programmable Gate Arrays (FPGA), based on the information received at the CTP from the FEBs. The L2 trigger serves as a *Camera Trigger*, so that the digitized pixel content, stored in the FEB buffers, is read-out and sent to the DAQ system at the Counting House. The main purpose of the L2 trigger is to further reduce the camera's DAQ rate based on the output of the L1 trigger. This *Camera Trigger* is based on 2 steps, the so-called Local Level 2 Trigger and Topo-Stereo trigger Level 2 Trigger [12].

Local L2 Trigger. The specific algorithm for generating the Local L2 trigger signal is still under discussion. Two main approaches are considered: an unsupervised clustering algorithm, namely the Density-Based Spatial Clustering of Applications with Noise (DBSCAN) algorithm [13], and another option based on Convolution Neural Networks (CNN) [14].

Local L2 Trigger: DBSCAN. The DBSCAN algorithm is a natural choice for distinguishing signal from background when searching for slight increases in photon density in part of the camera relative to the NSB. It efficiently identifies dense clusters of arbitrary shape in a multidimensional space. The algorithm requires two input parameters, *Eps, MinPts*. For the distance metric, we chose the Euclidean metric. The *Eps* and *MinPts* define least dense cluster in the data: *Eps*-Neighborhood

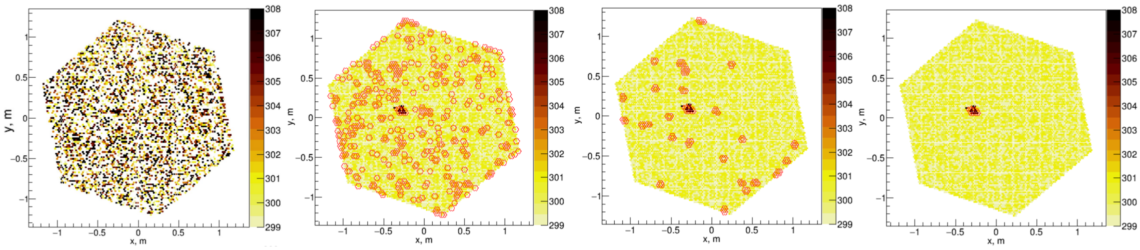

Figure 3: The 12 GeV on-axis gamma ray with a core located 180 m from the telescope. We plot the instantaneous ADC value of the digitized waveform by selecting the time frame with the maximum signal. (**First left**): The nominal NSB rate is 268 MHz/channel, and the nominal electronic noise 3.94 ADC counts RMS. (**Second left**): The NSB rate is set to 0, and the electronic noise is set to 0.1 RMS ADC counts. The fine red lines indicate the contours of the flower-like pattern where the digital sum exceeds the threshold, superimposed over the entire readout interval. (**First right**): Only spatially coincident flowers are shown. (**Second right**): Only flowers that are spatially and temporally coincident are shown. Note: simulations with a 268 MHz/channel NSB rate and an electronic noise level of 3.94 ADC are used in the analysis, with visualizations superimposed on noise-free waveforms.

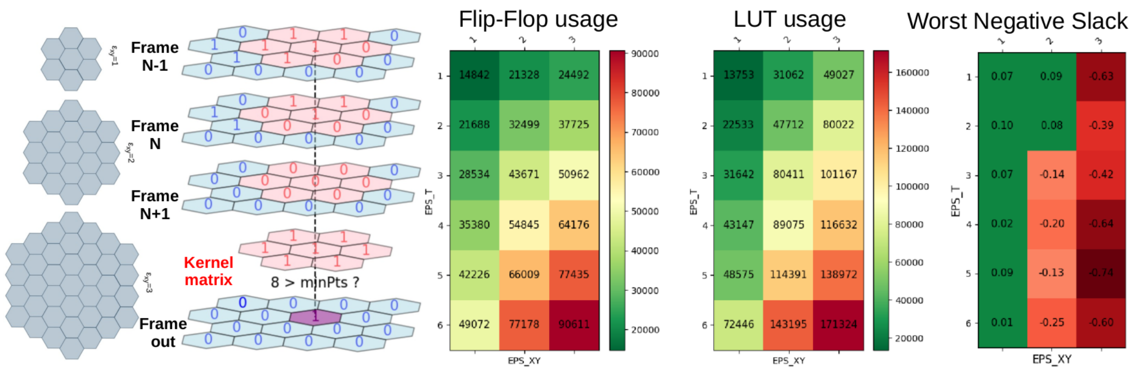

Figure 4: TDSCAN algorithm and FPGA implementation. (**Left**): Kernel sizes used for convolution. (**Center**): Hexagonal 3D convolution over two spatial coordinates and one temporal dimension (frames N-1, N, N+1 ...), producing the output frame. (**Right**): Resource usage and timing at 350 MHz target frequency.

contains at least *MinPts* points. Both of them can be defined manually, but the approximate *Eps* value is often determined using a sorted k-distance graph [13]. This method can be routinely used for image cleaning, however applying it to the time sequence, as we record waveforms, requires scaling the time dimension relative to the two spatial axes representing the channel positions in the camera. Figure 3 illustrates DBSCAN's ability to analyze waveforms, successfully detecting a 12 GeV gamma ray.

In the context of AdvCam, DBSCAN will be fed with the L1 signals from the 1171 7-pixel flowers. It is currently considered as the primary option for the Local L2 Trigger, as DBSACAN-like algorithms can run in the CTP FPGAs to cope with the 1 GHz input rate, thus requiring no L1 filter in the FEBs. Additionally, DBSCAN can provide the shower position in the camera, to be later used for the Topo-Stereo L2 trigger.

Local L2 Trigger: TDSCAN. We propose an FPGA-efficient approximation of DBSCAN that uses 3D convolution with a hexagonal kernel. TDSCAN stand for Trigger Distributed Spatial

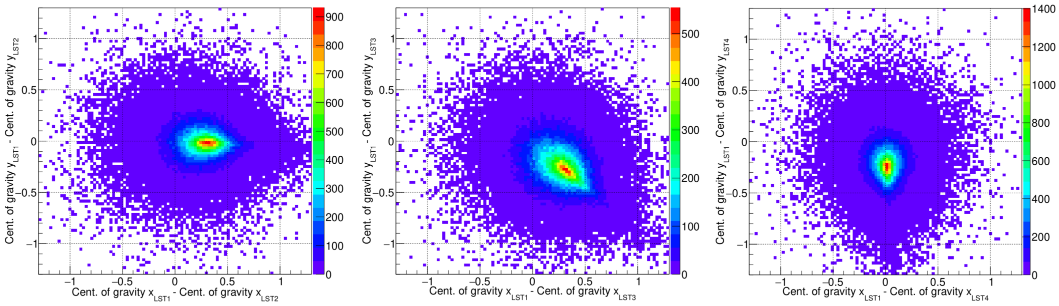

Figure 5: The differences in camera signal barycenters for proton events between LST-1 and other LSTs: LST-2 (left), LST-3 (center), and LST-4 (right).

Convolution Accelerator Network (Figure 4). It has three hyperparameters: Eps_t, Eps_{XY}, and *MinPts*, where *Eps* is defined separately for the temporal and spatial dimensions. The algorithm does not differentiate between different clusters and has a fixed latency for a given Eps_t, Eps_{XY}, making it suitable for working with data streams. The TDSCAN algorithm works in simulation and has been implemented on the Xilinx KCU105 board. It can run at a frequency of **350 MHz** with a latency of approximately **14.28 ns** (Eps_t=1, Eps_{XY}=1), and 1 GHz version in development.

Local L2 Trigger: Convolutional Neural Networks. CNN is a special type of Deep Neural Networks, especially effective at handling 2D images, as demonstrated by the `CTLearn` [15] package for IACT offline reconstruction [16]. These networks consist of convolutional layers combined with pooling layers. The convolutional layers apply filters that extract features (like edges, shapes, and textures). In contrast, the pooling layers perform sub-sampling to maintain key features and spatial relationships between pixels, thus enhancing the network's efficiency and minimizing memory requirements. Finally, fully connected layers provide high-level reasoning based on the extracted feature maps, leading to the final prediction.

CNN algorithms can process full-camera raw waveforms, of 5–10 ns long, to distinguish NSB from showers, or gammas from hadrons. They also provide shower position candidates for the Topo-Stereo L2 trigger. Once optimized for CTP FPGAs, they are a viable option for the Local L2 Trigger algorithm. However, the expected maximum inference rate for CNN L2 Trigger algorithms is about 1 MHz. This requires using an L1 trigger filter at the FEB level to reduce the rate from 1 GHz to 1 MHz, based on a simple digital sum cut.

Topo-Stereo L2 Trigger. Once an AdvCam has produced a Local L2 Trigger signal it is shared with the rest of the cameras of the LST array, so that at each camera CTP a Topo-Stereo L2 trigger is evaluated. The corresponding Stereo L2 trigger is thus considered the *Camera Trigger*, providing the desired data acquisition system (DAQ) rate of ~40-50 kHz. Figure 5 illustrates the topological trigger principle: knowing the shower position in one telescope allows us to predict its location in the other three telescopes. This effectively reduces false stereo coincidences.

Level 3 trigger The L2 trigger logic ensures that a minimum of two AdvCams are read out for each detected event. Following this, a Level-3 (L3) software-based trigger is applied within the DAQ system, enabling the real-time processing of raw waveforms from all read-out cameras. We use `CTLearn`, a high-level IACT data analysis package, to implement a simple CNN (~200k model parameters) with three convolutional layers (32, 32, 64 filters) and a dense head (256, 64

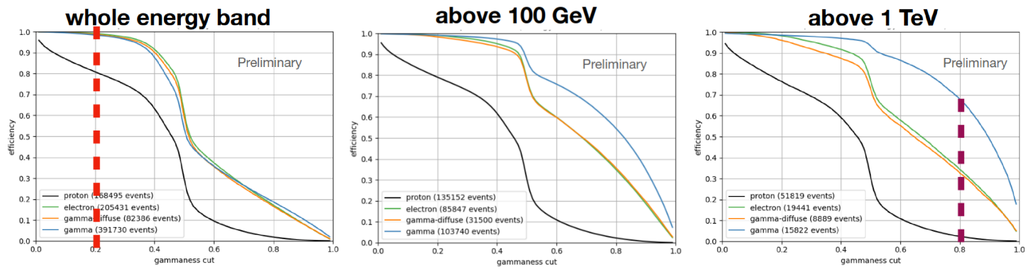

Figure 6: Efficiency curves for on-axis gamma rays, diffuse gamma rays, electrons, and protons as a function of the classifier output (gammaness). The three panels correspond to different energy ranges: whole energy band (**left**), above 100 GeV (**middle**), and above 1 TeV (**right**).

neurons) for binary classification. By porting a comparable `CTLearn` model to the OpenVINO framework, we achieved real-time inference at ~40k frames per second on an Intel Arria 10 PAC FPGA, matching the desired DAQ rate. The applied floating point (FP) precision reduction from FP32 to FP16 preserved the physics performance at $O(10^{-3})$. Further precision reductions (FP12, INT9, INT8) are under study and also the usage of quantization-aware training via `hls4ml` [17] to minimize a potential performance drop is planned.

This L3 software-based trigger approach offers the ability of real-time suppressing of proton-like cosmic-ray events. Cosmic rays are the dominant background occurring up to $\sim 10^5$ times more frequently than gamma rays (depending on observational conditions). Thereby, this approach can reduce data storage and computational demands downstream. In the left panel of Fig. 6, the red vertical line indicates a very loose gammaness cut that preserves nearly all gamma rays and electrons while reducing data volume by 20% (rejection of protons), demonstrating the model's utility for online triggering. In the right panel of Fig. 6, the purple line marks a cut that retains ~70% of on-axis gammas above 1 TeV, a typical benchmark for optimizing high-level off-line analysis selections. Notably, the model effectively rejects nearly all protons above 1 TeV while maintaining an on-axis gamma-ray efficiency of ~70%, highlighting its strong background suppression capabilities in the high-energy regime. Across the whole energy range, this cut rejects more than half of the simulated proton events.

5. Results and conclusions

We present a comparison of the trigger collection area as a function of gamma-ray energy for the current LST-1 [18] and a simulation of the AdvCam using the newly proposed trigger scheme on Figure 7 (left). As expected, the enhancement is more significant in the low-energy range, which is primarily the responsibility of LSTs. The AdvCam, with its novel readout system, can significantly enhance the triggering capabilities of a single LST. The DBSCAN algorithm has great potential not only for providing a sophisticated trigger but also for cleaning the data cube.

We present the trigger efficiency of the Local L2 CNN-based trigger scheme as a function of the number of detected p.e. The CNNs have been trained on simulated camera *patches*, i.e., portions of the camera with 7 superflowers (343 pixels), containing either NSB-induced or NSB and shower-induced p.e. *Shower-ness* refers to the classifier values returned by the trained CNN for distinguishing between shower and NSB events. For each camera patch, a *shower-ness* score

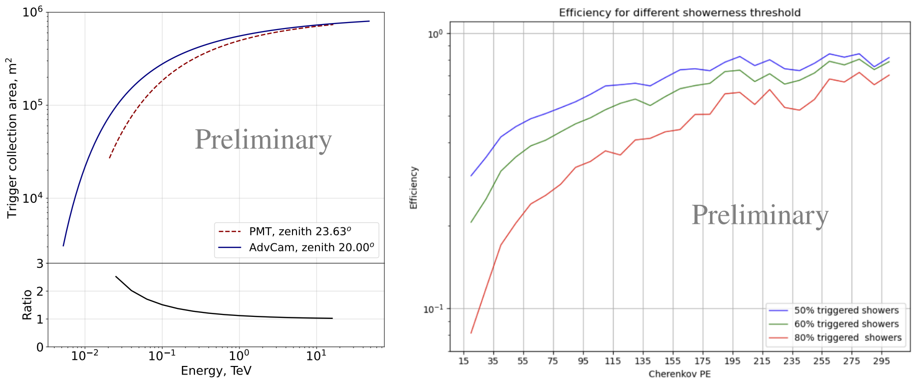

Figure 7: (**Left**): (**Preliminary**) Trigger collection area as a function of gamma energy for the current LST-1 and the AdvCam with the newly proposed trigger scheme and corresponding ratio between the two configurations. (**Right**): Trigger efficiency as a function of the number of p.e. per event for the single CNN model, applying 3 different cuts in the predicted showerness value.

is computed, and a full event trigger is determined by applying a logical OR operation across all predictions. Figure 7 (right) displays the results for three different thresholds applied to the showerness value predicted by the CNN. These thresholds correspond to different levels of stringency, defined by the percentage of triggered events that are actual showers (i.e., the ratio of shower triggers to total triggers). Despite its simplicity, the single CNN model demonstrates the ability to effectively distinguish between patches dominated by NSB and those containing real shower signals. Notably, the trigger shows strong performance even at low p.e. counts. In addition, the use of hexagonal convolution, the lightweight architecture, and ongoing efforts toward model size reduction make this CNN trigger scheme a promising candidate for implementation on FPGAs.

References

[1] B.S. Acharya et al. doi:10.1016/j.astropartphys.2013.01.007.

[2] A.M. Hillas. *Astropar. Phys.*, 43:19–43, 2013.

[3] N. Mythra et al. Nuv-hd sipms with metal-filled trenches. 2024.

[4] M. Heller et al. *The Euro. Phys. Jour. C*, 77:1–31, 2017.

[5] L. Burmistrov et al. doi:10.3390/instruments8010013.

[6] L. Burmistrov et al. doi:10.1051/epjconf/202328306006.

[7] H. Heller et al. In *38th Int. Cos. Ray Conf.*, volume 444, page 740, 2023.

[8] D. Heck et al. Corsika: A monte carlo code to simulate extensive air showers. *Report fzka*, 6019(11), 1998.

[9] Konrad Bernlöhr. *Astroparticle Physics*, 30(3):149–158, 2008.

[10] DAMPE collaboration. *Science advances*, 5(9):eaax3793, 2019.

[11] J. Aleksić et al. doi:10.1016/j.jheap.2015.01.002.

[12] R. López-Coto et al. doi:10.1088/1748-0221/11/04/p04005.

[13] M. Ester et al. volume 96, pages 226–231, 1996.

[14] Y. LeCun et al. Gradient-based learning applied to document recognition.

[15] T. Miener et al. doi:10.5281/zenodo.15065761.

[16] T. Miener et al. doi:10.22323/1.395.0730.

[17] J. Duarte et al. doi:10.1088/1748-0221/13/07/p07027.

[18] H. Abe et al. doi:10.3847/1538-4357/ace89d.

Full Author List: CTAO-LST Project

K. Abe[1], S. Abe[2], A. Abhishek[3], F. Acero[4,5], A. Aguasca-Cabot[6], I. Agudo[7], C. Alispach[8], D. Ambrosino[9], F. Ambrosino[10], L. A. Antonelli[10], C. Aramo[9], A. Arbet-Engels[11], C. Arcaro[12], T.T.H. Arnesen[13], K. Asano[2], P. Aubert[14], A. Baktash[15], M. Balbo[8], A. Bamba[16], A. Baquero Larriva[17,18], V. Barbosa Martins[19], U. Barres de Almeida[20], J. A. Barrio[17], L. Barrios Jiménez[13], I. Batkovic[12], J. Baxter[2], J. Becerra González[13], E. Bernardini[12], J. Bernete[21], A. Berti[11], C. Bigongiari[10], E. Bissaldi[22], O. Blanch[23], G. Bonnoli[24], P. Bordas[6], G. Borkowski[25], A. Briscioli[26], G. Brunelli[27,28], J. Buces[17], A. Bulgarelli[27], M. Bunse[29], I. Burelli[30], L. Burmistrov[31], M. Cardillo[32], S. Caroff[14], A. Carosi[10], R. Carraro[10], M. S. Carrasco[26], F. Cassol[26], D. Cerasole[33], G. Ceribella[11], A. Cerviño Cortínez[17], Y. Chai[11], K. Cheng[2], A. Chiavassa[34,35], M. Chikawa[2], G. Chon[11], L. Chytka[36], G. M. Cicciari[37,38], A. Cifuentes[21], J. L. Contreras[17], J. Cortina[21], H. Costantini[26], M. Croisonnier[23], M. Dalchenko[31], P. Da Vela[27], F. Dazzi[10], A. De Angelis[12], M. de Bony de Lavergne[39], R. Del Burgo[9], C. Delgado[21], J. Delgado Mengual[40], M. Dellaiera[14], D. della Volpe[31], B. De Lotto[30], L. Del Peral[41], R. de Menezes[34], G. De Palma[22], C. Díaz[21], A. Di Piano[27], F. Di Pierro[34], R. Di Tria[33], L. Di Venere[42], D. Dominis Prester[43], A. Donini[10], D. Dorner[44], M. Doro[12], L. Eisenberger[44], D. Elsässer[45], G. Emery[26], L. Feligioni[26], F. Ferrarotto[46], A. Fiasson[14,47], L. Foffano[32], F. Frías García-Lago[13], S. Fröse[45], Y. Fukazawa[48], S. Gallozzi[10], R. Garcia López[13], S. Garcia Soto[21], C. Gasbarra[49], D. Gasparrini[49], J. Giesbrecht Paiva[20], N. Giglietto[22], F. Giordano[33], N. Godinovic[50], T. Gradetzke[45], R. Grau[23], L. Greaux[19], D. Green[11], J. Green[11], S. Gunji[51], P. Günther[44], J. Hackfeld[19], D. Hadasch[2], A. Hahn[11], M. Hashizume[48], T. Hassan[21], K. Hayashi[52,2], L. Heckmann[11,53], M. Heller[31], J. Herrera Llorente[13], K. Hirotani[2], D. Hoffmann[26], D. Horns[15], J. Houles[26], M. Hrabovsky[36], D. Hrupec[54], D. Hui[55,2], M. Iarlori[56], R. Imazawa[48], T. Inada[2], Y. Inome[2], S. Inoue[57,2], K. Ioka[58], M. Iori[46], T. Itokawa[2], A. Iuliano[9], J. Jahanvi[30], I. Jimenez Martinez[11], J. Jimenez Quiles[23], I. Jorge Rodrigo[21], J. Jurysek[59], M. Kagaya[52,2], O. Kalashev[60], V. Karas[61], H. Katagiri[62], D. Kerszberg[23,63], M. Kherlakian[19], T. Kiyomot[64], Y. Kobayashi[2], K. Kohri[65], A. Kong[2], P. Kornecki[7], H. Kubo[2], J. Kushida[1], B. Lacave[31], M. Lainez[17], G. Lamanna[14], A. Lamastra[10], L. Lemoigne[14], M. Linhoff[45], S. Lombardi[10], F. Longo[66], R. López-Coto[7], M. López-Moya[17], A. López-Oramas[13], S. Loporchio[33], A. Lorini[3], J. Lozano Bahilo[41], F. Lucarelli[10], H. Luciani[66], P. L. Luque-Escamilla[67], P. Majumdar[68,2], M. Makariev[69], M. Mallamaci[37,38], D. Mandat[59], M. Manganaro[43], D. K. Maniadakis[10], G. Manicò[38], K. Mannheim[44], S. Marchesi[28,27,70], F. Marini[12], M. Mariotti[12], P. Marquez[71], G. Marsella[38,37], J. Martí[67], O. Martinez[72,73], G. Martínez[21], M. Martínez[23], A. Mas-Aguilar[17], M. Massa[3], G. Maurin[14], D. Mazin[2,11], J. Méndez-Gallego[7], S. Menon[10,74], E. Mestre Guillen[75], D. Miceli[12], T. Miener[17], J. M. Miranda[72], R. Mirzoyan[11], M. Mizote[76], T. Mizuno[48], M. Molero Gonzalez[13], E. Molina[13], T. Montaruli[31], A. Moralejo[23], D. Morcuende[7], A. Moreno Ramos[72], A. Morselli[49], V. Moya[17], H. Muraishi[77], S. Nagataki[78], T. Nakamori[51], C. Nanci[27], A. Neronov[60], D. Nieto Castaño[17], M. Nievas Rosillo[13], L. Nikolic[3], K. Nishijima[1], K. Noda[57,2], D. Nosek[79], V. Novotny[79], S. Nozaki[2], M. Ohishi[2], Y. Ohtani[2], T. Oka[80], A. Okumura[81,82], R. Orito[83], L. Orsini[3], J. Otero-Santos[7], P. Ottanelli[84], M. Palatiello[10], G. Panebianco[27], D. Paneque[11], F. R. Pantaleo[22], R. Paoletti[3], J. M. Paredes[6], M. Pech[59,36], M. Pecimotika[23], M. Peresano[11], F. Pfeifle[44], E. Pietropaolo[56], M. Pihet[6], G. Pirola[11], C. Plard[14], F. Podobnik[3], M. Polo[21], E. Prandini[12], M. Prouza[59], S. Rainò[33], R. Rando[12], W. Rhode[45], M. Ribó[6], V. Rizi[56], G. Rodriguez Fernandez[49], M. D. Rodríguez Frías[41], P. Romano[24], A. Roy[48], A. Ruina[12], E. Ruiz-Velasco[14], T. Saito[2], S. Sakurai[2], D. A. Sanchez[14], H. Sano[85,2], T. Šarić[50], Y. Sato[86], F. G. Saturni[10], V. Savchenko[60], F. Schiavone[33], B. Schleicher[44], F. Schmuckermaier[11], F. Schussler[39], T. Schweizer[11], M. Seglar Arroyo[23], T. Siegert[44], G. Silvestri[12], A. Simongini[10,74], J. Sitarek[25], V. Sliusar[8], I. Sofia[34], A. Stamerra[10], J. Strišković[54], M. Strzys[2], Y. Suda[48], A. Sunny[10,74], H. Tajima[81], M. Takahashi[81], J. Takata[2], R. Takeishi[2], P. H. T. Tam[2], S. J. Tanaka[86], D. Tateishi[64], T. Tavernier[59], P. Temnikov[69], Y. Terada[64], K. Terauchi[80], T. Terzic[43], M. Teshima[11,2], M. Tluczykont[15], F. Tokanai[51], T. Tomura[2], D. F. Torres[75], F. Tramonti[3], P. Travnicek[59], G. Tripodo[38], A. Tutone[10], M. Vacula[36], J. van Scherpenberg[11], M. Vázquez Acosta[13], S. Ventura[3], S. Vercellone[24], G. Verna[3], I. Viale[12], A. Vigliano[30], C. F. Vigorito[34,35], E. Visentin[34,35], V. Vitale[49], V. Voitsekhovskyi[31], G. Voutsinas[31], I. Vovk[2], T. Vuillaume[14], R. Walter[8], L. Wan[2], J. Wójtowicz[25], T. Yamamoto[76], R. Yamazaki[86], Y. Yao[1], P. K. H. Yeung[2], T. Yoshida[62], T. Yoshikoshi[2], W. Zhang[75], The CTAO-LST Project

[1]Department of Physics, Tokai University, 4-1-1, Kita-Kaname, Hiratsuka, Kanagawa 259-1292, Japan. [2]Institute for Cosmic Ray Research, University of Tokyo, 5-1-5, Kashiwa-no-ha, Kashiwa, Chiba 277-8582, Japan. [3]INFN and Università degli Studi di Siena, Dipartimento di Scienze Fisiche, della Terra e dell'Ambiente (DSFTA), Sezione di Fisica, Via Roma 56, 53100 Siena, Italy. [4]Université Paris-Saclay, Université Paris Cité, CEA, CNRS, AIM, F-91191 Gif-sur-Yvette Cedex, France. [5]FSLAC IRL 2009, CNRS/IAC, La Laguna, Tenerife, Spain. [6]Departament de Física Quàntica i Astrofísica, Institut de Ciències del Cosmos, Universitat de Barcelona, IEEC-UB, Martí i Franquès, 1, 08028, Barcelona, Spain. [7]Instituto de Astrofísica de Andalucía-CSIC, Glorieta de la Astronomía s/n, 18008, Granada, Spain. [8]Department of Astronomy, University of Geneva, Chemin d'Ecogia 16, CH-1290 Versoix, Switzerland. [9]INFN Sezione di Napoli, Via Cintia, ed. G, 80126 Napoli, Italy. [10]INAF - Osservatorio Astronomico di Roma, Via di Frascati 33, 00040, Monteporzio Catone, Italy. [11]Max-Planck-Institut für Physik, Boltzmannstraße 8, 85748 Garching bei München. [12]INFN Sezione di Padova and Università degli Studi di Padova, Via Marzolo 8, 35131 Padova, Italy. [13]Instituto de Astrofísica de Canarias and Departamento de Astrofísica, Universidad de La Laguna, C. Vía Láctea, s/n, 38205 La Laguna, Santa Cruz de Tenerife, Spain. [14]Univ. Savoie Mont Blanc, CNRS, Laboratoire d'Annecy de Physique des Particules - IN2P3, 74000 Annecy, France. [15]Universität Hamburg, Institut für Experimentalphysik, Luruper Chaussee 149, 22761 Hamburg, Germany. [16]Graduate School of Science, University of Tokyo, 7-3-1 Hongo, Bunkyo-ku, Tokyo 113-0033, Japan. [17]IPARCOS-UCM, Instituto de Física de Partículas y del Cosmos, and EMFTEL Department, Universidad Complutense de Madrid, Plaza de Ciencias, 1. Ciudad Universitaria, 28040 Madrid, Spain. [18]Faculty of Science and Technology, Universidad del Azuay, Cuenca, Ecuador.. [19]Institut für Theoretische Physik, Lehrstuhl IV: Plasma-Astroteilchenphysik, Ruhr-Universität Bochum, Universitätsstraße 150, 44801 Bochum, Germany. [20]Centro Brasileiro de Pesquisas Físicas, Rua Xavier Sigaud 150, RJ 22290-180, Rio de Janeiro, Brazil. [21]CIEMAT, Avda. Complutense 40, 28040 Madrid, Spain. [22]INFN Sezione di Bari and Politecnico di Bari, via Orabona 4, 70124 Bari, Italy. [23]Institut de Fisica d'Altes Energies (IFAE), The Barcelona Institute of Science and Technology, Campus UAB, 08193 Bellaterra (Barcelona), Spain. [24]INAF - Osservatorio Astronomico di Brera, Via Brera 28, 20121 Milano, Italy. [25]Faculty of Physics and Applied Informatics, University of Lodz, ul. Pomorska 149-153, 90-236 Lodz, Poland. [26]Aix Marseille Univ, CNRS/IN2P3, CPPM, Marseille, France. [27]INAF - Osservatorio di Astrofisica e Scienza dello spazio di Bologna, Via Piero Gobetti 93/3, 40129 Bologna, Italy. [28]Dipartimento di Fisica e Astronomia (DIFA) Augusto Righi, Università di Bologna, via Gobetti 93/2, I-40129 Bologna, Italy. [29]Lamarr Institute for Machine Learning and Artificial Intelligence, 44227 Dortmund, Germany. [30]INFN Sezione di Trieste and Università degli studi di Udine, via delle scienze 206, 33100 Udine, Italy. [31]University of Geneva - Département de physique nucléaire et corpusculaire, 24 Quai Ernest Ansernet, 1211 Genève 4, Switzerland. [32]INAF - Istituto di Astrofisica e Planetologia Spaziali (IAPS), Via del Fosso del Cavaliere 100, 00133 Roma, Italy. [33]INFN Sezione di Bari and Università di Bari, via Orabona 4, 70126 Bari, Italy. [34]INFN Sezione di Torino, Via P. Giuria 1, 10125 Torino, Italy. [35]Dipartimento di Fisica - Universitá degli Studi di Torino, Via Pietro Giuria 1 - 10125 Torino, Italy. [36]Palacky University Olomouc, Faculty of Science, 17. listopadu 1192/12, 771 46 Olomouc, Czech Republic. [37]Dipartimento di Fisica e Chimica 'E. Segrè' Università degli Studi di Palermo, via delle Scienze, 90128 Palermo. [38]INFN Sezione di Catania, Via S. Sofia 64, 95123 Catania, Italy. [39]IRFU, CEA, Université Paris-Saclay, Bât 141, 91191 Gif-sur-Yvette, France. [40]Port d'Informació Científica, Edifici D, Carrer de l'Albareda, 08193 Bellaterrra (Cerdanyola del Vallès), Spain. [41]University of Alcalá UAH, Departamento de Physics and Mathematics, Pza. San Diego, 28801, Alcalá de Henares, Madrid, Spain. [42]INFN Sezione di Bari, via Orabona 4, 70125, Bari, Italy. [43]University of Rijeka, Department of Physics, Radmile Matejcic 2, 51000 Rijeka, Croatia. [44]Institute for Theoretical Physics and Astrophysics, Universität Würzburg, Campus Hubland Nord, Emil-Fischer-Str. 31, 97074 Würzburg, Germany. [45]Department of Physics, TU Dortmund University, Otto-Hahn-Str. 4, 44227 Dortmund, Germany. [46]INFN Sezione di Roma La Sapienza, P.le Aldo Moro, 2 - 00185 Rome, Italy. [47]ILANCE, CNRS – University of Tokyo International Research Laboratory, University of Tokyo, 5-1-5 Kashiwa-no-Ha Kashiwa City, Chiba 277-8582, Japan. [48]Physics Program, Graduate School of Advanced Science and Engineering, Hiroshima University, 1-3-1 Kagamiyama, Higashi-Hiroshima City, Hiroshima, 739-8526, Japan. [49]INFN Sezione di Roma Tor Vergata, Via della Ricerca Scientifica 1, 00133 Rome, Italy. [50]University of Split, FESB, R. Boškovića 32, 21000 Split, Croatia. [51]Department of Physics, Yamagata University, 1-4-12 Kojirakawa-machi, Yamagata-shi, 990-8560, Japan. [52]Sendai College, National Institute of Technology, 4-16-1 Ayashi-Chuo, Aoba-ku, Sendai city, Miyagi 989-3128, Japan. [53]Université Paris Cité, CNRS, Astroparticule et Cosmologie, F-75013 Paris, France. [54]Josip Juraj Strossmayer University of Osijek, Department of Physics, Trg Ljudevita Gaja 6, 31000 Osijek, Croatia. [55]Department of Astronomy and Space Science, Chungnam National University, Daejeon 34134, Republic of Korea. [56]INFN Dipartimento di Scienze Fisiche e Chimiche - Università degli Studi dell'Aquila and Gran Sasso Science Institute, Via Vetoio 1, Viale Crispi 7, 67100 L'Aquila, Italy. [57]Chiba University, 1-33, Yayoicho,

Inage-ku, Chiba-shi, Chiba, 263-8522 Japan. [58]Kitashirakawa Oiwakecho, Sakyo Ward, Kyoto, 606-8502, Japan. [59]FZU - Institute of Physics of the Czech Academy of Sciences, Na Slovance 1999/2, 182 21 Praha 8, Czech Republic. [60]Laboratory for High Energy Physics, École Polytechnique Fédérale, CH-1015 Lausanne, Switzerland. [61]Astronomical Institute of the Czech Academy of Sciences, Bocni II 1401 - 14100 Prague, Czech Republic. [62]Faculty of Science, Ibaraki University, 2 Chome-1-1 Bunkyo, Mito, Ibaraki 310-0056, Japan. [63]Sorbonne Université, CNRS/IN2P3, Laboratoire de Physique Nucléaire et de Hautes Energies, LPNHE, 4 place Jussieu, 75005 Paris, France. [64]Graduate School of Science and Engineering, Saitama University, 255 Simo-Ohkubo, Sakura-ku, Saitama city, Saitama 338-8570, Japan. [65]Institute of Particle and Nuclear Studies, KEK (High Energy Accelerator Research Organization), 1-1 Oho, Tsukuba, 305-0801, Japan. [66]INFN Sezione di Trieste and Università degli Studi di Trieste, Via Valerio 2 I, 34127 Trieste, Italy. [67]Escuela Politécnica Superior de Jaén, Universidad de Jaén, Campus Las Lagunillas s/n, Edif. A3, 23071 Jaén, Spain. [68]Saha Institute of Nuclear Physics, A CI of Homi Bhabha National Institute, Kolkata 700064, West Bengal, India. [69]Institute for Nuclear Research and Nuclear Energy, Bulgarian Academy of Sciences, 72 boul. Tsarigradsko chaussee, 1784 Sofia, Bulgaria. [70]Department of Physics and Astronomy, Clemson University, Kinard Lab of Physics, Clemson, SC 29634, USA. [71]Institut de Fisica d'Altes Energies (IFAE), The Barcelona Institute of Science and Technology, Campus UAB, 08193 Bellaterra (Barcelona), Spain. [72]Grupo de Electronica, Universidad Complutense de Madrid, Av. Complutense s/n, 28040 Madrid, Spain. [73]E.S.CC. Experimentales y Tecnología (Departamento de Biología y Geología, Física y Química Inorgánica) - Universidad Rey Juan Carlos. [74]Macroarea di Scienze MMFFNN, Università di Roma Tor Vergata, Via della Ricerca Scientifica 1, 00133 Rome, Italy. [75]Institute of Space Sciences (ICE, CSIC), and Institut d'Estudis Espacials de Catalunya (IEEC), and Institució Catalana de Recerca I Estudis Avançats (ICREA), Campus UAB, Carrer de Can Magrans, s/n 08193 Bellatera, Spain. [76]Department of Physics, Konan University, 8-9-1 Okamoto, Higashinada-ku Kobe 658-8501, Japan. [77]School of Allied Health Sciences, Kitasato University, Sagamihara, Kanagawa 228-8555, Japan. [78]RIKEN, Institute of Physical and Chemical Research, 2-1 Hirosawa, Wako, Saitama, 351-0198, Japan. [79]Charles University, Institute of Particle and Nuclear Physics, V Holešovičkách 2, 180 00 Prague 8, Czech Republic. [80]Division of Physics and Astronomy, Graduate School of Science, Kyoto University, Sakyo-ku, Kyoto, 606-8502, Japan. [81]Institute for Space-Earth Environmental Research, Nagoya University, Chikusa-ku, Nagoya 464-8601, Japan. [82]Kobayashi-Maskawa Institute (KMI) for the Origin of Particles and the Universe, Nagoya University, Chikusa-ku, Nagoya 464-8602, Japan. [83]Graduate School of Technology, Industrial and Social Sciences, Tokushima University, 2-1 Minamijosanjima,Tokushima, 770-8506, Japan. [84]INFN Sezione di Pisa, Edificio C – Polo Fibonacci, Largo Bruno Pontecorvo 3, 56127 Pisa, Italy. [85]Gifu University, Faculty of Engineering, 1-1 Yanagido, Gifu 501-1193, Japan. [86]Department of Physical Sciences, Aoyama Gakuin University, Fuchinobe, Sagamihara, Kanagawa, 252-5258, Japan.

Acknowledgments

We gratefully acknowledge financial support from the following agencies and organisations: Conselho Nacional de Desenvolvimento Científico e Tecnológico (CNPq), Fundação de Amparo à Pesquisa do Estado do Rio de Janeiro (FAPERJ), Fundação de Amparo à Pesquisa do Estado de São Paulo (FAPESP), Fundação de Apoio à Ciência, Tecnologia e Inovação do Paraná - Fundação Araucária, Ministry of Science, Technology, Innovations and Communications (MCTIC), Brasil; Ministry of Education and Science, National RI Roadmap Project DO1-153/28.08.2018, Bulgaria; Croatian Science Foundation (HrZZ) Project IP-2022-10-4595, Rudjer Boskovic Institute, University of Osijek, University of Rijeka, University of Split, Faculty of Electrical Engineering, Mechanical Engineering and Naval Architecture, University of Zagreb, Faculty of Electrical Engineering and Computing, Croatia; Ministry of Education, Youth and Sports, MEYS LM2023047, EU/MEYS CZ.02.1.01/0.0/0.0/16_013/0001403, CZ.02.1.01/0.0/0.0/18_046/0016007, CZ.02.1.01/0.0/0.0/16_019/0000754, CZ.02.01.01/00/22_008/0004632 and CZ.02.01.01/00/23_015/0008197 Czech Republic; CNRS-IN2P3, the French Programme d'investissements d'avenir and the Enigmass Labex, This work has been done thanks to the facilities offered by the Univ. Savoie Mont Blanc - CNRS/IN2P3 MUST computing center, France; Max Planck Society, German Bundesministerium für Bildung und Forschung (Verbundforschung / ErUM), Deutsche Forschungsgemeinschaft (SFBs 876 and 1491), Germany; Istituto Nazionale di Astrofisica (INAF), Istituto Nazionale di Fisica Nucleare (INFN), Italian Ministry for University and Research (MUR), and the financial support from the European Union – Next Generation EU under the project IR0000012 - CTA+ (CUP C53C22000430006), announcement N.3264 on 28/12/2021: "Rafforzamento e creazione di IR nell'ambito del Piano Nazionale di Ripresa e Resilienza (PNRR)"; ICRR, University of Tokyo, JSPS, MEXT, Japan; JST SPRING - JPMJSP2108; Narodowe Centrum Nauki, grant number 2023/50/A/ST9/00254, Poland; The Spanish groups acknowledge the Spanish Ministry of Science and Innovation and the Spanish Research State Agency (AEI) through the government budget lines PGE2022/28.06.000X.711.04, 28.06.000X.411.01 and 28.06.000X.711.04 of PGE 2023, 2024 and 2025, and grants PID2019-104114RB-C31, PID2019-107847RB-C44, PID2019-104114RB-C32, PID2019-105510GB-C31, PID2019-104114RB-C33, PID2019-107847RB-C43, PID2019-107847RB-C42, PID2019-107988GB-C22, PID2021-124581OB-I00, PID2021-125331NB-I00, PID2022-136828NB-C41, PID2022-137810NB-C22, PID2022-138172NB-C41, PID2022-138172NB-C42, PID2022-138172NB-C43, PID2022-139117NB-C41, PID2022-139117NB-C42, PID2022-139117NB-C43, PID2022-139117NB-C44, PID2022-136828NB-C42, PDC2023-145839-I00 funded by the Spanish MCIN/AEI/10.13039/501100011033 and "and by ERDF/EU and NextGenerationEU PRTR; the "Centro de Excelencia Severo Ochoa" program through grants no. CEX2019-000920-S, CEX2020-001007-S, CEX2021-001131-S; the "Unidad de Excelencia María de Maeztu" program through grants no. CEX2019-000918-M, CEX2020-001058-M; the "Ramón y Cajal" program through grants RYC2021-032991-I funded by MICIN/AEI/10.13039/501100011033 and the European Union "NextGenerationEU"/PRTR and RYC2020-028639-I; the "Juan de la Cierva-Incorporación" program through grant no. IJC2019-040315-I and "Juan de la Cierva-formación"' through grant JDC2022-049705-I. They also acknowledge the "Atracción de Talento" program of Comunidad de Madrid through grant no. 2019-T2/TIC-12900; the project "Tecnologías avanzadas para la exploración del universo y sus componentes" (PR47/21 TAU), funded by Comunidad de Madrid, by the Recovery, Transformation and Resilience Plan from the Spanish State, and by NextGenerationEU from the European Union through the Recovery and Resilience Facility; "MAD4SPACE: Desarrollo de tecnologías habilitadoras para estudios del espacio en la Comunidad de Madrid" (TEC-2024/TEC-182) project funded by Comunidad de Madrid; the La Caixa Banking Foundation, grant no. LCF/BQ/PI21/11830030; Junta de Andalucía under Plan Complementario de I+D+I (Ref. AST22_0001) and Plan Andaluz de Investigación, Desarrollo e Innovación as research group FQM-322; Project ref. AST22_00001_9 with funding from NextGenerationEU funds; the "Ministerio de Ciencia, Innovación y Universidades" and its "Plan de Recuperación, Transformación y Resiliencia"; "Consejería de Universidad, Investigación e Innovación" of the regional government of Andalucía and "Consejo Superior de Investigaciones Científicas", Grant CNS2023-144504 funded by MICIU/AEI/10.13039/501100011033 and by the European Union NextGenerationEU/PRTR, the European Union's Recovery and Resilience Facility-Next Generation, in the framework of the General Invitation of the Spanish Government's public business entity Red.es to participate in talent attraction and retention programmes within Investment 4 of Component 19 of the Recovery, Transformation and Resilience Plan; Junta de Andalucía under Plan Complementario de I+D+I (Ref. AST22_00001), Plan Andaluz de Investigación, Desarrollo e Innovación (Ref. FQM-322). "Programa Operativo de Crecimiento Inteligente" FEDER 2014-2020 (Ref. ESFRI-2017-IAC-12), Ministerio de Ciencia e Innovación, 15% co-financed by Consejería de Economía, Industria, Comercio y Conocimiento del Gobierno de Canarias; the "CERCA" program and the grants 2021SGR00426 and 2021SGR00679, all funded by the Generalitat de Catalunya; and the European Union's NextGenerationEU (PRTR-C17.I1). This research used the computing and storage resources provided by the Port d'Informació Científica (PIC) data center. State Secretariat for Education, Research and Innovation (SERI) and Swiss National Science Foundation (SNSF), Switzerland; The research leading to these results has received funding from the European Union's Seventh Framework Programme (FP7/2007-2013) under grant agreements No 262053 and No 317446; This project is receiving funding from the European Union's Horizon 2020 research and innovation programs under agreement No 676134; ESCAPE - The European Science Cluster of Astronomy & Particle Physics ESFRI Research Infrastructures has received funding from the European Union's Horizon 2020 research and innovation programme under Grant Agreement no. 824064.